Vailable online at www.sciencedirect.com

SciVerse ScienceDirect

Energy Procedia 27 (2012) 95 – 102

Energy Procedia

SiliconPV: April 03-05, 2012, Leuven, Belgium

Analysis and optimization of the bulk and rear recombination of screen-printed PERC solar cells

S. Gatz[a]*, J. Müller[a], T. Dullweber[a]**, and R. Brendel[a,b]

[a] *Institute for Solar Energy Hamelin (ISFH), Am Ohrberg 1, 31860 Emmerthal, Germany*

[b] Institute for Solid-State Physics, Leibniz Universität Hannover, Appelstrasse 2, 30167 Hannover, Germany

Abstract

In this paper, we investigate the impact of the rear surface passivation, the silicon base material and the local aluminum contacts applied to rear side passivated solar cells with a homogenously doped emitter at the front. We compare different dielectric surface passivation layers (SiO_2, Al_2O_3, SiN_x) on a high-efficiency level using 125×125 mm^2 and 156×156 mm^2 *p*-type Cz silicon wafers. It turns out that applying an Al_2O_3/SiN_x layer stack outperforms all other surface passivation layers due to its excellent surface passivation as well as optical properties. We determine the impact of the light induced degradation depending on the used Cz base material. We measure an efficiency drop between 0.0 % (Ga-doped) and 0.8 % abs. (B-doped) after 8 hours of illumination under 0.5 Suns. We measure the surface recombination velocity of local screen-printed Al contacts with varying the metallisation fraction f_{rear} with the dynamic infrared lifetime mapping technique (dyn-ILM) on lifetime samples. We measure a decrease in contact recombination velocity from above 1100 cm/s for small f_{rear} to 400 cm/s for large f_{rear} on 1.5 Ωcm *p*-type FZ-silicon. Microscopy investigations show that this is due to an improved local Al-BSF formation when using higher f_{rear}.

Keywords: Photovoltaics; Silicon; Solar Cells; Surface Passivation

1. Introduction

Industrial crystalline Si solar cells typically feature a full-area aluminum (Al) back surface field (BSF) at the rear. It provides a good ohmic contact and a moderate rear side passivation with effective rear

* now with SolarWorld Innovations GmbH, Berthelsdorfer Str. 111 A, 09599 Freiberg, Germany

** Corresponding author, Tel.: +49-5151-999-638; fax: +49-5151-999-400, *E-mail address*: t.dullweber@isfh.de

doi:10.1016/j.egypro.2012.07.035

surface recombination velocities S_{rear} ranging from 200 to 600 cm/s on 2-4 Ωcm *p*-type silicon [1,2]. In order to increase the cell efficiency, the passivation quality at the rear has to be improved. A dielectric layer at the rear also improves the internal reflectivity and hence the infrared light absorption of the solar cell.

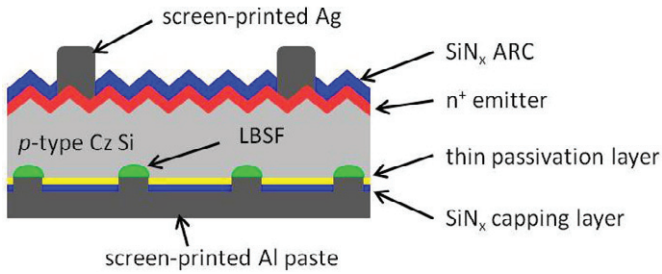

Fig. 1. Schematic of PERC solar cells with screen-printed Ag front and Al rear contacts. We analyse different passivation layers, *p*-type Cz-Si base materials and the impact of the rear local contact opening width.

This paper compares different rear passivation layers such as SiO_2/SiN_x, Al_2O_3/SiN_x, SiN_x. The light-induced degradation is investigated depending on dopant type. The formation of local Al screen-printed contacts in the passivation layer and its impact on the recombination velocity of the contacts S_{met} have been investigated before [3]. In contrast to Ref. 3 we do observe a significant influence of the metallisation fraction f_{rear} on S_{met}. The f_{rear} is in this paper defined as the fraction between metallised line width after firing and pitch p. We observe a correlation between S_{met} and the contact broadening during firing.

2. Investigation of rear surface passivation layers

Tab. 1. Solar cell parameters measured under standard testing conditions using ~180 µm-thick, *p*-type Cz-silicon, PERC design with identical rear side contact structure and $f_{rear} \approx 10$ % (No. 1-3, 5) using boron-doped ρ = 2.1 Ωcm (No. 1-4) and Ga-doped ρ = 0.7 Ωcm Cz-Si (No. 5).

No.	Rear passivation	Area [cm^2]	f_{rear} [%]	Dopant	V_{oc} [mV]	J_{sc} [mA/cm^2]	*FF* [%]	η [%]	$\eta_{illuminated}$ (%)
1	SiO_2/SiN_x	233	10	boron	652	38.3	77.2	19.3	18.5
2	Al_2O_3/SiN_x	149	10	boron	646	39.0	77.2	19.5	
3	SiN_x	149	10	boron	642	38.3	77.4	19.1	
4	Al-BSF	147	100	boron	632	37.1	79.8	18.7	
5	SiO_2/SiN_x	233	10	gallium	657	37.6	77.3	19.1	19.1

We apply different passivation layers to our PERC solar cell process with a homogeneous emitter and Ag screen-printed front contacts [4]. We compare on the basis of solar cell results three types of industrially relevant passivation layers: a thermally-grown SiO_2 capped with plasma enhanced chemical vapour deposited (PECVD) SiN_x, a stack of plasma-assisted (PA) ALD-Al_2O_3 /SiN_x and a SiN_x single layer. The passivation layer thickness is in the range of 5-30 nm, the SiN_x layer thickness is in the range of 100-250 nm. On *p*-type FZ-Silicon test wafers with ρ = 1.5 Ωcm, these passivation layers show a surface recombination velocity $S_{pass} \leq 10$ cm/s for SiO_2/SiN_x [5] and ALD-Al_2O_3/SiN_x [6,7] at injection densities relevant for solar cell application ($\Delta n = 10^{13}$ - 10^{15} cm^{-3}). A SiN_x single layer shows a $S_{pass} \approx 50$ cm/s after firing for $\Delta n = 10^{15}$ cm^{-3} [8]. They are therefore promising candidates for the rear side passivation of screen-printed PERC solar cells. Conventional solar cells with a full area Al-BSF are

processed as reference. Table 1 shows the measured cell parameters of PERC solar cells with SiO_2/SiN_x (No. 1), PA ALD-Al_2O_3 /SiN_x (No. 2) and SiN_x rear side passivation (No. 3). A conventional solar cell with a full area Al-BSF is shown as reference (No. 4). Considering No. 1-3, solar cells with identical rear contact geometry are compared, which explains the similar *FF*. The impact of the passivation layers can be observed in the open-circuit voltage V_{oc} and the short-circuit current density J_{sc}. In order to compare the J_{sc} variation, the reflectivity *R* and the internal quantum efficiency (IQE) are measured as shown in Fig. 2.

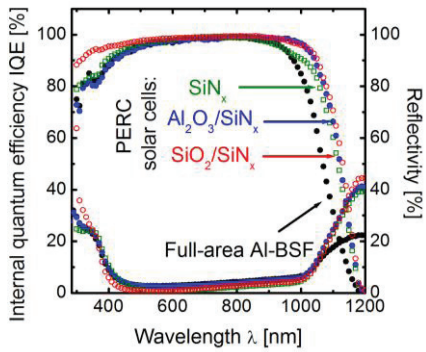

Fig. 2. Internal quantum efficiency (IQE) and reflectivity of screen-printed PERC solar cells with SiO_2/SiN_x (red), ALD-Al_2O_3 /SiN_x (blue) and SiN_x (green) rear side passivation compared to a conventional solar cell with full area Al-BSF (black).

The Al_2O_3/SiN_x (blue) and SiN_x (green) passivated PERC cells have a similar emitter doping profile and SiN_x front surface passivation as the full area Al-BSF solar cell (black). Therefore, both the IQE and reflectivity almost coincide in the short wavelength region. In contrast, the PERC solar cell with SiO_2/SiN_x rear and front passivation (red) show a deviation in the short wavelength reflectivity. Due to the fact that for both solar cells *R* and IQE almost coincidence in the long wavelength region, we conclude that the difference in the front side antireflection coating contribute to a lower short circuit current density for SiO_2/SiN_x (J_{sc}= 38.3 mA/cm^2) compared to Al_2O_3/SiN_x (J_{sc}= 39.0 mA/cm^2) passivated PERC solar cells. Only a part of the losses ($\leq$ 0.3 mA/cm^2) can be explained by the slightly higher front side shading at the 156×156 mm^2 solar cell No.1. However the IQE data which are adjusted for reflectivity show for the SiO_2/SiN_x passivation in the short wavelength region an increase. It results from a significantly lower phosphorus concentration at the surface caused by the thermal oxidation as shown in Ref. [9]. This explains the improved open-circuit voltage of cell No. 1 compared to cell 2 and 3 in Tab. 1.

In the long-wavelength region, the strong improvement of *R* and IQE are clearly shown to be due to the dielectric rear surface passivation. Using an IQE evaluation program from Fischer [10], based on models from Basore [11] and Brendel and Rau [12], the internal reflectance R_b and the effective rear surface recombination velocity S_{rear} are extracted from the wavelength region between 850 nm and 1000 nm. We assume a bulk lifetime τ_b = 800 µs, which we obtained on Cz *p*-type test samples in the regenerated state. The investigated layers show a R_b of about 90 %. The full area Al-BSF solar cell shows a S_{rear} = (450 ± 100) cm/s. All applied dielectric passivation layers show a decreased recombination at the rear. While S_{rear} = (70 ± 30) cm/s for Al_2O_3/SiN_x and S_{rear} = (90 ± 30) cm/s for SiO_2/SiN_x passivated solar cells, it is S_{rear} = (300 ± 80) cm/s for the SiN_x passivated PERC solar cell. Applying SiN_x passivation (cell No. 3 in Tab. 1) results therefore not only in a moderate V_{oc} = 642 mV but also in a moderate J_{sc} = 38.3 mA/cm^2 compared to V_{oc} = 646 mV and J_{sc} = 39.0 mA/cm^2 for the PERC solar cell with Al_2O_3/SiN_x passivation (No. 2). Thereby the increased S_{rear} is caused by the high injection dependency of the SiN_x surface passivation with $S_{pass} \geq$ 100 cm/s for $\Delta n = 10^{13}$ cm^{-3} on 1.5 Ωcm *p*-type FZ-Si wafers. In contrast, the SiO_2/SiN_x and Al_2O_3/SiN_x passivation layers do not depend on Δn in the relevant range 10^{13}-10^{15}cm^{-3}.

3. Investigation of different Si bulk materials on light induced degradation

The PERC solar cell No. 1 in Tab. 1 is illuminated for 8 hours with white light, which typically suffices to activate all recombination active boron-oxygen-complexes. Thus we measure a cell efficiency degradation of 0.8 % abs. to 18.5 % for the boron-doped Cz-Si. The effect of light induced degradation for boron-doped Cz-Si wafer is shown in Fig. 3. As shown in Fig. 3 a) the IQE and *R* are agreeing for small wavelengths λ, one can recognize in Fig. 3 b) that the data for λ > 850 nm differ during white light illumination. Using the software LASSIE [10,13] we extract from the IQE data for λ > 850 nm the effective surface recombination velocity S_{rear}, and the bulk diffusion length L_b. While for both the S_{rear} is supposed to be constant at (90 ± 30) cm/s, the extracted L_b decreases from 1940 µm (regenerated) to 490 µm (degraded). This corresponds to a bulk lifetime degradation from 1200 µs to 80 µs and fits well with obtained bulk lifetime on our test wafers of τ_b = 800 µs in the regenerated state compared to τ_b = 100 µs in the degraded state. For comparison purposes a solar cell was made with the same SiO_2/SiN_x passivation and the same screen-printing Al-paste applying a Ga-doped Cz-Si wafer with a base resistivity ρ = 0.7 Ωcm (cell No. 5 in Tab. 1). It suffers from a lower J_{sc} = 37.6 mA/cm^2 at about the same *FF* = 77.3 % and slightly increased V_{oc} = 657 mV resulting in η = 19.1 %. However, this PERC solar cell does not show any degradation during illumination. Therefore the IQE of the Ga-doped Cz-Si PERC solar cell does not alter at all during illumination. From the IQE data in the long wavelength region we extract S_{rear} = (200 ± 50) cm/s and L_b = (1150 ± 200) µm corresponding to a bulk lifetime τ_b = 490 µs. This fits very well with measured τ_b = 450 µs on test wafers before and after illuminating with white light.

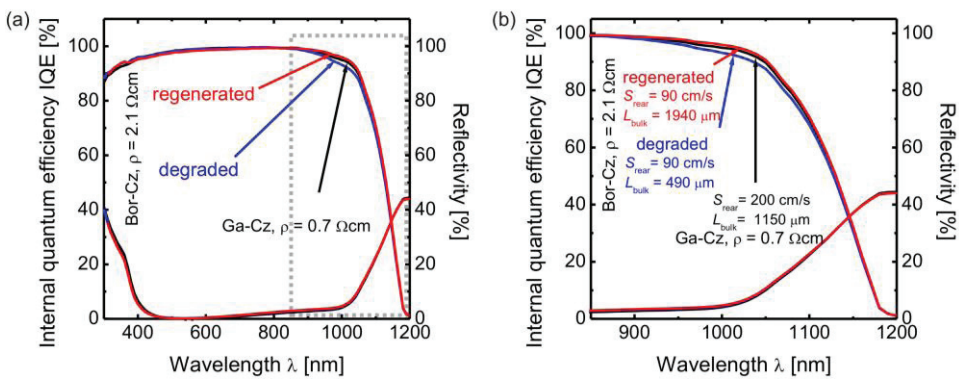

Fig. 3. a) Internal quantum efficiency (IQE) and reflectivity curves of SiO_2/SiN_x-passivated PERC solar cells on *p*-type Cz silicon. Applying Boron dopants results in different IQE curves depending on degraded (red) or regenerated status (blue). In contrast, the IQE curve of PERC solar cells applying Ga dopants does not change during annealing. b) Zoom-in to the wavelength range where S_{rear} and L_b are extracted using the software LASSIE [10,13].

4. Structural investigations of local Al-BSF and its influence on the surface recombination velocity

We study the formation of the solar cell rear contacts, which are fabricated by local laser ablation of the passivation stack followed by full-area Al screen-printing and firing. We measure the contact recombination velocity performing lifetime measurements on test samples. For this purpose we use 290 µm-thick, 125 mm × 125 mm *p*-type, boron-doped and shiny-etched Float-Zone silicon wafers with a resistivity of 1.5 Ωcm. The wafers are cleaned in a wet chemical RCA process. A dry thermal oxidation is carried out resulting in a 10 nm-thick SiO_2 layer on both surfaces. Afterwards we deposit symmetrically SiN_x layers with an in-line microwave PECVD system. At one side, the SiO_2/SiN_x passivation stacks are locally ablated by a 532 nm laser with pulse lengths of 10 picoseconds (**L**aser **C**ontact **O**penings). We

vary the metallisation fraction at the rear f_{rear} by varying the local LCO area as well as the pitch p. The metallisation is realized by full-area Al screen-printing using the same Al paste as for the cells in Tab. 1. The samples are fired in a belt furnace at a nominal peak set temperature between 870°C and 930 °C and a belt velocity of 5.9 m/min.

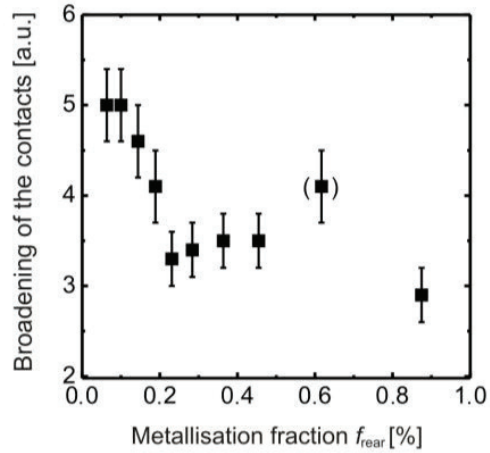

Fig. 4. Structural investigations of the screen-printed local Al BSF contact formation to the base: broadening of the contact width as a function of the metallization fraction f_{rear}.

Due to the local alloying process of Si and Al in local contacts a broadening of the screen-printed contact geometry compared to the dielectric ablated geometry has been reported before [14]. Fig. 4 plots the broadening of the contact structure as a function of the f_{rear}. It is provided by comparing the LCO fraction f_{LCO} after laser ablation with the metallisation fraction f_{rear} after firing. The f_{LCO} is determined by measuring the local LCO area using optical microscope images after the laser ablation. The f_{rear} is determined by measuring the width of the contact cross section using scanning electron microscopy images. There is a steep decrease of the broadening up to f_{rear} = 0.2 % and thus to a certain contact opening width. By a further increase of the contact opening structure, the contact broadening saturates.

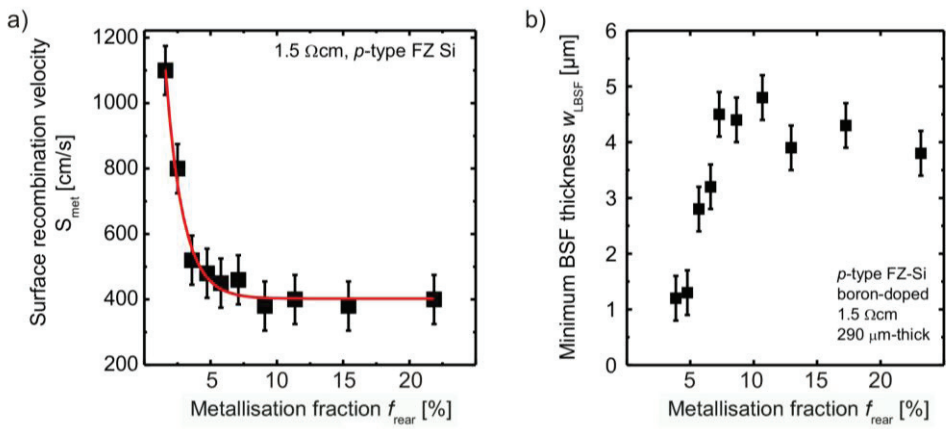

Fig. 5. a) Decreased surface recombination velocity of the metallised contacts S_{met} with increased metallisation fraction up to f_{rear} = 5 % following by a saturation in S_{met} = (400 ± 75) cm/s. b) The minimum BSF thickness strongly depends on f_{rear} for $f_{rear} \leq 7$ % and saturates at about 4 µm for $f_{rear} > 7$µm.

Applying the calibration-free dynamic infrared carrier lifetime mapping (dyn-ILM) technique [15] we obtain mappings of the effective lifetime τ_{eff}. Using the approach in Ref. [16] we obtain an upper limit for

the area-averaged rear surface recombination velocity S_{rear} for each single contact geometry window. In order to determine the surface recombination velocity in the metallised areas S_{met} we use the equation developed by Fischer [10,17,18] that describes the area-averaged S_{rear} as a function of S_{met} and S_{pass} which is the surface recombination velocity in the passivated areas. As shown in Figure 5 a) a decrease of S_{met} from (1100 ± 100) cm/s down to (400 ± 75) cm/s is observed with increased metallisation fraction up to f_{rear} = 5 %, whereby the pitch between the line contacts remains constant. The constant S_{met} for f_{rear} > 5 % demonstrates that the contact opening matters only up to a certain limit. Figure 4 b) shows the minimum Al-BSF width w_{LBSF} as a function of f_{rear}. The w_{LBSF} is the smallest Al p^+-doped thickness in the local contact, mostly measured at the contact edges. It is determined by means of secondary electron microscopy measurements. While w_{LBSF} is around 1 µm for small f_{rear}, it increases significantly with increasing f_{rear} and saturates at about 4 µm for f_{rear} > 7 %.

Figure 6 shows the correlation between the measured S_{met} from Fig. 5 a) and the measured minimum Al-BSF thickness w_{LBSF} in Fig. 5 b). The data clearly indicate that small w_{LBSF} lead to high contact recombination velocities S_{met}. According to the method introduced in Ref. [19], we perform a numerical simulation to verify the measured change in the recombination properties at specific contact schemes as a function of the Al-BSF layer thickness. The input parameters for the simulations are the base resistivity of 1.5 Ωcm, the bulk lifetime in the Al-p^+ layer τ_{bulk} = 130 ns [20] and the rear surface recombination velocity $S_{cell,rear} = 10^7$ cm/s. We use a depth dependent Al doping profile

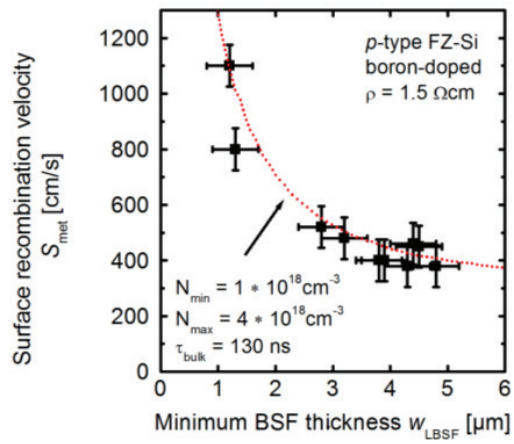

Fig. 6. Decreased surface recombination velocity S_{met} at the contacts with increased minimum BSF thickness w_{LBSF} corresponds to simulations (red dotted line)

$$N_{Al}(z) = N_{\min} \exp\left(\frac{z}{w_{LBSF}} \ln\left(\frac{N_{\max}}{N_{\min}}\right)\right) \quad (1)$$

in the Al-p^+ region of thickness w_{LBSF} with N_{min} = 1 × 10^{18} cm^{-3} and N_{max} = 4 × 10^{18} cm^{-3}, which is comparable to previously measured doping profiles of full area Al-p^+ layers [20]. The results of the simulations in Fig. 6 clearly confirm the experimental finding.

5. Conclusions

We have demonstrated an excellent optical and surface passivation performance of Al_2O_3/SiN_x layers at the rear side of fully screen-printed PERC solar cells with homogeneous phosphorus-doped front side emitter. The investigated alternative dielectric layers suffer either from a moderate rear surface passivation (SiN_x) or from an increased reflection on the solar cell front (SiO_2/SiN_x). In an investigation regarding the base material we observed a degradation of the efficiency during illumination of 0.8 % absolute using boron-doped Cz-Si. In contrast Ga-doped Cz-Si does not show any degradation resulting in an energy conversion efficiency of 19.1 % before and after illuminating. The influence of the

metallisation fraction f_{rear} on the surface recombination velocity below the metal contacts S_{met} is investigated in detail. We demonstrated S_{met} < 500 cm/s for large f_{rear} on lifetime samples with $\rho = 1.5\ \Omega$cm. The application of the improved rear contact geometry and Al_2O_3/SiN_x rear surface passivation contributes to a PERC solar cell efficiency of 20.1 %, with J_{sc} = 39.0 mA/cm^2, V_{oc} = 655 mV and *FF* = 78.8 % [21,22].

Acknowledgements

The authors thank U. Baumann, B. Beier, S. Dorn, O. Peters for sample and solar cell processing. This work was supported by the German Federal Ministry for the Environment, Nature Conservation and Nuclear Safety under Contract No. 0325296 in cooperation with Solland Solar Cells BV, SolarWorld Innovations GmbH, SCHOTT Solar AG, RENA GmbH and SINGULUS TECHNOLOGIES AG, which is gratefully acknowledged.

References

[1] S. Narasimha and A. Rohatgi, Optimized Al back surface field techniques for Si solar cells, *Proceedings 26th IEEE PVSC*, 1997, pp. 63–66

[2] S. Peters, Rapid Thermal Processing of Crystalline Silicon Materials and Solar Cells, *PhD thesis*, University Konstanz , 2004

[3] J.Mueller, K. Bothe, S. Gatz, H. Plagwitz, G. Schubert, and R. Brendel, "Contact formation and recombination at screen-printed local aluminum-alloyed Silicon solar cell base contacts", *IEEE Transaction on electron devices*, 58, no. 10, 2011, pp. 3239-3245

[4] T. Dullweber, S. Gatz, H. Hannebauer, T. Falcon, R. Hesse, J. Schmidt and R. Brendel, Towards 20% efficient large-area screen-printed rear-passivated silicon solar cells, *Progress in Photovoltaics: Research and Applications*, 2011, DOI: 10.1002/pip.1198

[5] J. Schmidt, M. Kerr, and A. Cuevas, Surface passivation of silicon solar cells using plasma-enhanced chemical-vapour-deposited SiN films and thin thermal SiO_2/plasma SiN stacks, *Semiconductor Science and Technology* **16**, 2001, pp. 164-170

[6] J. Schmidt, B. Veith, and R. Brendel, Effective surface passivation of crystalline silicon using ultrathin Al_2O_3 films and Al_2O_3/SiN_x stacks, *phys. stat. sol. (RRL)* **3**, 2009, pp. 287-289

[7] B. Veith, F. Werner, D. Zielke, R. Brendel, and J. Schmidt, Comparison of the thermal stability of single Al_2O_3 layers and Al_2O_3/SiN_x stacks for the surface passivation of silicon, *Energy Procedia* **8**, 2001, pp. 397–312

[8] S. Gatz, H. Plagwitz, P. P. Altermatt, B. Terheiden, and R. Brendel, Thermally stable surface passivation by a-Si:H / SiN double layers for crystalline silicon solar cells, *in Proceedings 23rd European Photovoltaic Solar Energy Conference and Exhibition*, 2008, pp. 1033-1035

[9] S. Gatz, H. Hannebauer, R. Hesse, F. Werner, A. Schmidt, T. Dullweber, J. Schmidt, K. Bothe, and R. Brendel, 19.4%-efficient large-area fully screen-printed silicon solar cells, *Phys. Status Solidi RRL*, 5, no. 4, 2011, pp. 147–149

[10] B. Fischer, Loss analysis of crystalline silicon solar cells using photoconductance and quantum efficiency measurements, *Ph.D. thesis*, University Konstanz, 2003

[11] P. A. Basore, Extended spectral analysis of internal quantum efficiency, *in Proceedings 23rd IEEE PVSC*, 1993, pp. 147–152

[12] R. Brendel and U. Rau, Effective diffusion lengths for minority carriers in solar cells as determined from internal quantum efficiency analysis, *Journal of Applied Physics* **85**, 1999, pp. 3634-3637

[13] www.pv-tools.de

[14] S. Gatz, T. Dullweber and R. Brendel, Evaluation of series resistance losses in screen-printed solar cells with local rear contacts, *IEEE Journal of Photovoltaics*, Vol 1, No. 1, 2011, pp. 37-42

[15] K. Ramspeck, S. Reissenweber, J. Schmidt, K. Bothe, and R. Brendel, Dynamic carrier lifetime imaging of silicon wafers using an ingrared-camera-base approach, *Appl. Phys. Lett.* **93** (10), 2008, pp. 102-104

[16] J. Müller, K. Bothe, S. Gatz, F. Haase, C. Mader and R. Brendel , "Recombination at laser-processed local base contacts by dynamic infrared lifetime mapping", *Journal of Applied Physics*. 108, 2010, p. 124513

[17] B. Gelmont and M. Shur, Spreading resistance of a round ohmic contact, *Solid-State Electron.*, 36, no. 2, 1993, pp. 143-146

[18] B. Gelmont, M. S. Shur, and R. J. Mattauch, Disk and stripe capacitance, *Solid-State Electron.*, 38, no. 3, 1995, pp. 731-734

[19] J. Müller, K. Bothe, S. Gatz, H. Plagwitz, G. Schubert, and R. Brendel, Contact formation and recombination at screen-printed local Aluminum-alloyed Silicon solar cell base contacts, *Trans. Electr. Dev.* , 58, no. 10, 2010, pp. 3239-3245

[20] J. Schmidt, N. Thiemann, R. Bock and R. Brendel, Recombination lifetimes in highly aluminum-doped silicon, *Journal of Applied Physics*, 106, 2009, 093707, DOI: 10.1063/1.3253742

[21] ISFH press release: 20.1%-efficient screen printed silicon solar cell with novel rear passivation layer, March 2012

[22] B. Veith, T. Dullweber, M. Siebert, C. Kranz, F. Werner, N.-P. Harder, J. Schmidt, B.F.P. Roos, T. Dippell, and R. Brendel, Comparison of ICP-AlO_x and ALD-Al_2O_3 layers for the rear surface passivation of c-Si Solar cells, in *Proceedings 2nd Silicon PV conference*, 2012, submitted.